Journal of Power Sources 196 (2011) 5299–5308

Contents lists available at ScienceDirect

Journal of Power Sources

journal homepage: www.elsevier.com/locate/jpowsour

Energy storage characterization for a direct methanol fuel cell hybrid system

J. Wilhelm*, H. Janßen, J. Mergel, D. Stolten

Forschungszentrum Jülich GmbH, Institute of Energy Research - Fuel Cells (IEF-3), 52425 Jülich, Germany

ARTICLE INFO

Article history:
Received 11 June 2010
Received in revised form 12 August 2010
Accepted 29 September 2010
Available online 8 October 2010

Keywords:
Hybridization
DMFC
System
Energy storage
Characterization

ABSTRACT

This paper describes the energy storage characterization for a direct methanol fuel cell (DMFC) hybrid system for light traction applications. In a first step, the DMFC stack and the energy storage were dimensioned. To dimension the energy storage, the required energy density and power density were calculated. These are influenced by the operating states of the vehicle as well as the highly fluctuating load profile. For this kind of application a high energy density as well as a high power density is needed. Therefore, super capacitors are not the energy storage of choice. As an alternative, suitable batteries were analyzed in terms of their behavior in the DMFC hybrid system. Therefore, a characterization procedure was developed consisting of five different tests. These tests were developed adapted to the requirements of the application. They help to characterize the battery in terms of energy content, high power capability during charge and discharge, thermal behavior and lifetime. The tests showed that all batteries have to be operated on a partial state of charge (pSOC) and a thermal management is very important. Especially lead-acid battery show an decrease in lifetime under a pSOC operation. Therefore, a lithium battery was identified as the suitable energy storage for the considered application.

1. Introduction

Direct methanol fuel cells (DMFCs) directly convert liquid methanol into electric energy. The basic principle and the process engineering of a DMFC are described in [1,2]. As methanol has a very high energy density, they are attractive for various applications. For example as replacements for batteries in light traction applications [3]. This results in a longer operating time. Furthermore, there is no need for battery recharging and spare batteries. In the literature some examples for DMFCs in light traction applications can be found. In the two 4-wheel electric scooters JuMOVe [2,4] and JuMOVe 2nd [5] the DMFC replaces the lead-acid traction battery. Another example is the electric vehicle StartLab, where the DMFC is used as a range extender [6]. The DMFC driven electric motorcycle FC-me is described in [7].

A market analysis showed that the best potential for DMFC systems in light traction applications lies in the material handling sector [8]. Our current project deals with the horizontal order picker in [9], which is a small fork-lift truck. Typically, a lead-acid battery is used for traction. The aim of the project is to replace the traction battery with a DMFC system while maintaining the same driving performance. Several fuel cell systems for fork-lift trucks have been developed in the last years. Three different classes of fork-lift trucks exist [10]. Systems for counterbalanced trucks (class 1) with a proton exchange membrane fuel cell (PEMFC) are described in [11–14]. For reach trucks (class 2) also several PEMFC systems exist. Details can be found in [12–14]. The rated power of fuel cell systems for class 1 and class 2 fork-lift trucks is between 10 kW and 30 kW. For pallet trucks, which belong to class 3, a rated power between 1 kW and 5 kW is needed. A PEMFC system for this kind of fork-lift trucks is described in [12]. As PEMFCs have a high power density, they have advantages for class 1 and class 2 fork-lift trucks. DMFCs have advantages when a high energy density is needed. This is the case for class 3 fork-lift trucks, which are normally used in a three-shift operation. DMFC systems for this class can be found in [15,16]. The horizontal order picker, which is the exemplary application in our project, is a class 3 fork-lift truck. In [16] details on the first and second prototype can be found.

This paper deals with a DMFC system for an horizontal order picker. As they have a highly fluctuating load profile (see Section 2), the DMFC has to be hybridized with an energy storage. The energy storage is used to cover the acceleration power and to store the braking power (see Section 3). In the literature several concepts for the coupling of the fuel cell and the energy storage in such a fuel cell hybrid system exist. In [17] the fuel cell is directly coupled with a battery and/or a super capacitor. The indirect coupling is done with DC–DC converters. For one energy storage and one DC–DC converter either the fuel cell or the energy storage can be decoupled from the load (e.g. driving motor) via the DC–DC converter. For a battery these concepts are shown in [18], for a super capacitor in [19,20]. If the fuel cell and the energy storage are decoupled from the load, two DC–DC converters are needed [19,21]. A bat-

* Corresponding author. Tel.: +49 2461 611573; fax: +49 2461 616695.
E-mail address: j.wilhelm@fz-juelich.de (J. Wilhelm).

0378-7753/$ – see front matter © 2010 Elsevier B.V. All rights reserved.
doi:10.1016/j.jpowsour.2010.09.088

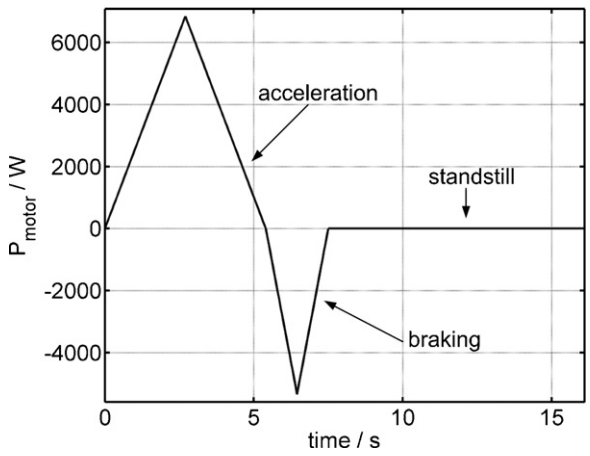

Fig. 1. Characteristic driving cycle.

tery and a super capacitor can be indirectly coupled with a fuel cell via two DC–DC converters [20] or three DC–DC converters [22]. Several of these hybridization concepts were analyzed in [23] with simulations and experiments.

The hybridization concept for the horizontal order picker will be described in Section 3. If the hybridization concept is known, the selection of a suitable energy storage will be the next step. Firstly the energy storage will be dimensioned in terms of energy and power density (see Section 4.2). Secondly several energy storages will be characterized (see Section 6). Therefore, a new characterization procedure adapted to the requirements of the application was developed (see Section 5).

2. Characteristic driving cycle

An exemplary application is the horizontal order picker in [9], which is normally used in large warehouses for material handling applications. The typical operation can be described by the characteristic driving cycle in Fig. 1. The characteristic driving cycle consists of the three phases: acceleration ($P_{motor} > 0$), braking ($P_{motor} < 0$) and standstill ($P_{motor} = 0$). During a typical three shift operation this driving cycle is repeated continuously without any breaks.

The driving cycle in Fig. 1 is an approximation based on long-term driving tests in a large warehouse as described in [23]. The results of the driving tests are the maximum amplitude and the maximum duration of the acceleration and braking peaks as shown in Table 1. For the characteristic driving cycle, these peaks are approximated with triangles as shown in Fig. 1. During standstill, the approximated power consumption is zero.

In Table 2 the average and the maximum driving power of the vehicle are shown. The average driving power $P_{driving,avg}$ is the average of the power profile in Fig. 1. The calculated value of 800 W can also be found in the data sheet of the application [9]. Compared to the high power values for acceleration and braking in Table 1, the average driving power is very moderate. This difference comes from the long standstill phase, where the vehicle stops to be loaded with different goods. When the vehicle is driven according to this characteristic driving cycle, this is called normal operation. However, the vehicle can also be driven at maximum speed. During this constant driving, the maximum driving power $P_{driving,max}$ is 2400 W [9]. This is called abnormal operation.

Table 1
Power value and duration for the three phases of the driving cycle.

Phase	Power (W)	Duration (s)
Acceleration	6800	5.4
Braking	−5300	2.1
Standstill	0	8.6

Table 2
Average and maximum driving power.

Parameter	Power (W)
Average driving power	800
Maximum driving power	2400

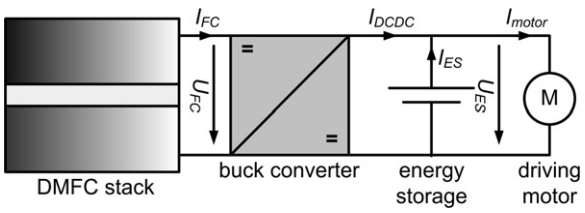

Fig. 2. DMFC hybrid system setup.

3. Hybridization concept

The aim is to build a DMFC system which has the same performance as the original traction battery. The following reasons are the motivation to hybridize the fuel cell with an energy storage:

- limited dynamic behavior of the fuel cell [19]
- need for energy recovery during braking [22]
- size reduction of the fuel cell [24]
- traction power during fuel cell start-up [25]

For the hybridization, several concepts are possible (see Section 1). Basically, series hybrid systems can be divided into the following two groups [26]:

- passive hybrids: direct coupling of fuel cell and energy storage
- active hybrids: indirect coupling of fuel cell and energy storage via converters

In Section 1 a literature review on different hybridization concepts was presented. On the basis of this literature review, several of these concepts were analyzed in [23]. Therefore, four basic hybridization concepts were identified. They were characterized with simulations and experiments. According to the criteria of system efficiency, required fuel cell power and dynamic behavior of the fuel cell, an active series hybrid with a buck converter between the fuel cell (FC) and the energy storage (ES) is the best concept for this application [23,27]. The resulting system setup can be seen in Fig. 2. The buck converter steps down the fuel cell voltage U_{FC}, resulting in a converter output voltage that is equal to the energy storage voltage U_{ES}. The output current I_{DCDC} of the buck converter is controlled [28]. As the converter is unidirectional, I_{DCDC} is always >0, whereas the energy storage current I_{ES} and the motor current I_{motor} can have both directions as shown in Table 3.

Table 3
Direction of energy storage and motor current.

Parameter	>0	<0
I_{ES}	Discharge	Charge
I_{motor}	Acceleration	Braking

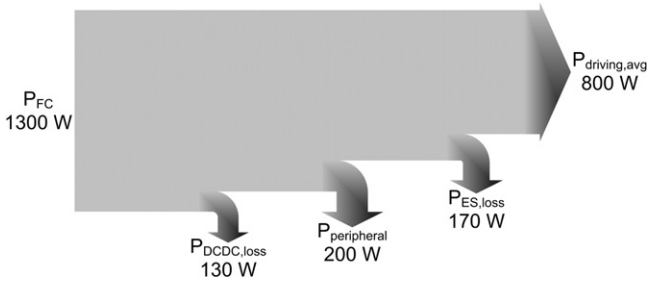

Fig. 3. Energy flow diagram.

4. Dimensioning of DMFC stack and energy storage

4.1. DMFC stack dimensioning

The main goal of the control strategy is to maintain the state of charge of the energy storage on a constant level [28]. To reach this goal, the useable electric power from the DMFC hybrid system should be equal to the average driving power $P_{driving,avg}$ shown in Table 2. Calculating backwards, the required fuel cell power P_{FC} can be expressed as:

$$P_{FC} = P_{driving,avg} + P_{peripheral} + P_{ES,loss} + P_{DCDC,loss} \quad (1)$$

In addition to the driving power, the power consumption of the peripheral components $P_{peripheral}$ must be covered. A DMFC system needs several peripheral components (e.g. pumps, blowers) as described in [28]. The power consumption of each component is known from the data sheet. In the worst-case the overall power consumption of the peripheral components is 200 W. As there are losses in the DMFC hybrid system, they also have to be taken into consideration. Electrical power losses exist at the energy storage ($P_{ES,loss}$) and the buck converter ($P_{DCDC,loss}$). Losses of the energy storage include the charge and discharge losses. The power losses were determined by simulations using the efficiency of the buck converter and the energy efficiency of the energy storage [23]. With the average driving power according to Table 2, the energy flow diagram in Fig. 3 shows how P_{FC} is calculated. The indicated power values represent the average values of the energy flows. As a result, the required DMFC stack power is 1300 W.

4.2. Energy storage dimensioning

As the DMFC stack delivers the average driving power, the main task of the energy storage is to cover the peak power during acceleration and to store the peak power during braking. The dimensioning parameters are the minimum energy content and the maximum power (charge and discharge). They are used to calculate the minimum energy density ED_{min} and the minimum power density PD_{min}. These dimensioning parameters are influenced by the following operating states of the vehicle:

- state 1: start-up
- state 2: normal operation
- state 3: abnormal operation

Parameters of these operating states are shown in Table 4. These three operating states have different influences on the dimensioning parameters ED_{min} and PD_{min}. In the following these influences will be described basically, whereas detailed calculations can be found in [23].

During start-up (state 1) the DMFC stack is heated up. The heating-up of the DMFC stack last about 20 minutes. To avoid aging of the fuel cell, the maximum fuel cell power is limited depending on the actual fuel cell temperature. This limitation is implemented in the control strategy [23,28]. As an assumption, the fuel cell power is set here to P_{FC} = 0 W during heating-up. In Table 4, two cases are distinguished for the motor power P_{motor} during start-up. As described in Table 2, the vehicle can be driven according to the characteristic driving cycle ($P_{motor} = P_{driving,avg} = 800$ W) or at its maximum driving power ($P_{motor} = P_{driving,max} = 2400$ W). As there is no power output from the DMFC stack, the driving power for the motor only comes from the energy storage (ES), thus resulting in a discharge. Additionally, also the power consumption of the peripheral components must be covered by the energy storage. This is the case for all operating states. Simulations in [23] were carried out to calculate the energy storage powers $P_{ES,1a}$ and $P_{ES,1b}$ for both cases of this operating state. The integration of $P_{ES,1a}$ and $P_{ES,1b}$ results in the minimum required energies $E_{ES,min,1a}$ and $E_{ES,min,1b}$, which will be used to calculate ED_{min}.

Table 4
Operating states of the vehicle.

State	P_{motor} (W)	P_{FC} (W)	Duration	Driving power from ...
1 a	800	0	20 min	ES
1 b	2400	0	20 min	ES
2	800	1300	24 h	FC + ES
3	2400	1300	10 min	FC + ES

During normal operation (state 2), the vehicle is driven according to the characteristic driving cycle (see Section 2). Theoretically, for this operating state the duration is only limited by the size of the methanol tank. As an assumption the vehicle could be operated according to the characteristic driving cycle for 24 h without refueling. The motor power in Table 4 is the same as for state 1 a, whereas the DMFC stack delivers its maximum power as described in Section 4.1. If the DMFC stack delivers its maximum power and the vehicle is driven according to the characteristic driving cycle, the energy storage will stay at a fixed state of charge (see Section 4.1). This results in a very small depth of discharge, which is described by the minimum required energy $E_{ES,min,2}$ for this operating state. $E_{ES,min,2}$ is calculated in the same way as for operating state 1.

In state 3, the vehicle is driven at its maximum driving power according to Table 2. This is called abnormal operation (see Section 2). This operating state is only allowed for 10 minutes. The DMFC stack power is the same as in state 2. As the driving power of the motor is higher than the average driving power, which was the basis for the DMFC stack dimensioning in Section 4.1, the difference has to be delivered by the energy storage. The discharge of the energy storage can be expressed by calculating the minimum required energy $E_{ES,min,3}$ for this operating state. This is done in the same way as for operating state 1.

The influence on the minimum power density PD_{min} depends on the driving cycle of the vehicle. For the calculation of the minimum power density PD_{min} only the peak power during discharge is taken into consideration. If the vehicle is driven according to the characteristic driving cycle (state 1 a and state 2), the maximum peak power during charging and discharging of the energy storage are similar to the acceleration and braking power of the driving cycle in Table 1 diminished by the DMFC stack power according to Table 4. Additionally, the consumption of the peripheral components is taken into consideration for this calculation. The maximum discharge powers $P_{ES,max,1a}$ and $P_{ES,max,2}$ for the energy storage were thus calculated [23]. If the vehicle is driven at its maximum driving power (state 1 b and state 3), there is no acceleration and braking as the vehicle drives with constant speed. Therefore, there is no peak power demand for the energy storage ($P_{ES,max,1b} = P_{ES,max,3} = 0$ W).

To calculate the minimum energy and power density, the maximum available space for the energy storage $V_{ES,max}$ is needed. The complete DMFC system has to fit into the original battery box of the horizontal order picker [16]. For some components the required

Table 5
Performance limits for the energy storage.

Parameter	Value
ED_{min}	65 Wh l^{-1}
PD_{min}	350 W l^{-1}

space is fixed. The calculated DMFC stack power (see Section 4.1) defines the volume of the DMFC stack and the size of the buck converter. The corresponding losses of the DMFC stack define the size of the condenser. The volume of the tank is variable in contrast and defines the range of the vehicle. In [16], the complete system setup is described. For an optimized design, the maximum available space for the energy storage is 20 l. Therefore, ED_{min} and PD_{min} are calculated using Eqs. (2) and (3). The results of these two calculations are shown in Table 5.

$$ED_{min} = \frac{max\left(E_{ES,min,1a}, E_{ES,min,1b}, E_{ES,min,2}, E_{ES,min,3}\right)}{V_{ES,max}} \quad (2)$$

$$PD_{min} = \frac{max\left(P_{ES,max,1a}, P_{ES,max,1b}, P_{ES,max,2}, P_{ES,max,3}\right)}{V_{ES,max}} \quad (3)$$

For the decision regarding which kind of energy storage is suitable for this application, a Ragone chart is used. The basis for the Ragone chart is a market analysis of available energy storages, which was conducted in [23]. The Ragone chart with the performance limits according to Table 5 can be seen in Fig. 4. It becomes clear that the energy density of super capacitors is too small, whereas batteries could have a suitable energy and power density. These batteries are indicated with the gray rectangle in Fig. 4. For the characterization in the following sections, three suitable batteries were chosen.

5. Characterization procedure

5.1. Motivation

The Ragone chart in Fig. 4 gives a first clue as to which battery could be used as an energy storage. In addition to the described performance limits ED_{min} and PD_{min} several aspects are important

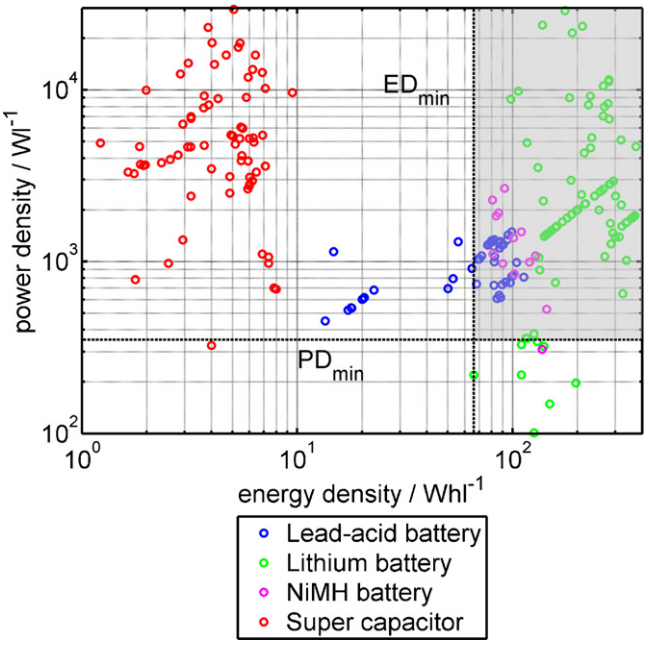

Fig. 4. Ragone chart with performance limits.

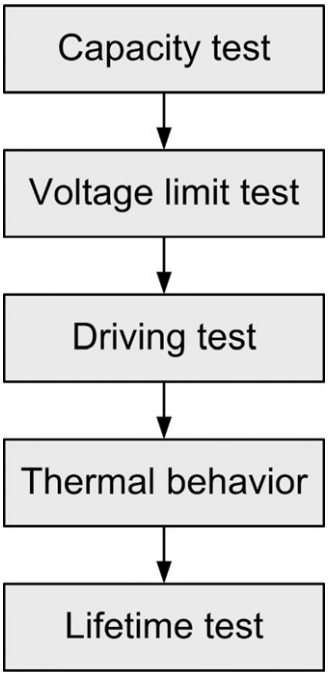

Fig. 5. Characterization procedure.

for the use of a battery in the desired application. The following questions should therefore be answered in advance:

- Is the energy content dependent on the discharge current?
- What is the maximum state of charge (SOC) range in which the battery could be used?
- Is it possible to cover the start-up of the DMFC stack with the battery?
- What is the thermal behavior of the battery?
- Is there an influence on the battery lifetime under this operation mode?

To answer these questions, a characterization procedure was developed, which consists of the steps indicated in Fig. 5. The characteristics of the different characterization steps and why they were chosen will be explained in the following sections.

5.2. Capacity test

The Ragone chart in Fig. 4 is based on manufacturer data on the different energy storages. To calculate the energy density of a battery, the manufacturer performs a capacity test with a defined discharge current. For an ideal battery, the discharged capacity would be the same for different discharge currents. However, in reality there is a dependency on the discharge current [29]. This is called Peukert's law. To determine this dependency, different capacity tests with different discharge currents were performed for each battery. For this test an electronic load and a power supply were connected in parallel to the battery. At first the battery was fully charged using the constant voltage (CV)–constant current (CC) charging method. Afterwards the fully charged battery was discharged with a constant current using the electronic load. The result is the discharged energy E_{cap} for a discharge current I_{cap}.

5.3. Voltage limit test

As described in Section 4.2, the main task of the battery is to cover the peak power during acceleration and to store the peak

power during braking. The battery voltage U_{ES} will increase during braking (= charge) and will decrease during acceleration (= discharge). The voltage level of the DMFC system should always be $24\,V \pm 30\% = [16.8\,V, 31.2\,V]$. This has to do with the motor controller of the horizontal order picker, which needs a certain voltage and is set to failure mode otherwise. Therefore, it is important to know which is the maximum state of charge for charging the battery during braking without violating the maximum voltage level $U_{level,max} = 31.2\,V$. This operating point is defined by the maximum open circuit voltage $U_{ES,00,max}$. On the other hand, it is important to know which is the minimum state of charge for discharging the battery during acceleration without violating the minimum voltage level $U_{level,min} = 16.8\,V$. This operating point is defined by the minimum open circuit voltage $U_{ES,00,min}$.

A fully charged battery was thus operated with a cycle consisting of a sequence of an acceleration peak and a braking peak according to Table 1 followed by a no load phase. Therefore, the battery was connected in parallel with a power sink and a power source. The power sinks simulates the power consumption of the motor during acceleration, whereas the power source represents the braking. As the open circuit voltage needs some time to reach steady state, the no load phase for the voltage limit test is longer than the standstill of the characteristic driving cycle as defined in Table 1. At the end of the no load phase the open circuit voltage of the battery was measured, which will be described later.

The number of repetitions of this sequence is indicated with n. The minimum voltage $U_{ES,min,n}$ for each acceleration peak and the maximum voltage $U_{ES,max,n}$ for each braking peak were measured. The voltage at the end of each no load phase is the open circuit voltage $U_{ES,00,n}$ at that working point. The maximum operating range of the battery between $U_{ES,00,max}$ and $U_{ES,00,min}$ was determined as follows:

- Upper limit:

$$U_{ES,00,max} = U_{ES,00,n}, \quad \text{if } U_{ES,max,n} = U_{level,max} \tag{4}$$

- Lower limit:

$$U_{ES,00,min} = U_{ES,00,n}, \quad \text{if } U_{ES,min,n} = U_{level,min} \tag{5}$$

After each repetition of the defined cycle the relations in Eqs. (4) and (5) are checked. If the measured maximum voltage $U_{ES,max,n}$ is equal to the defined maximum voltage level $U_{level,max}$, the measured open circuit voltage $U_{ES,00,n}$ at that operating point is the requested maximum open circuit voltage $U_{ES,00,max}$. This is defined by Eq. (4). The requested minimum open circuit voltage $U_{ES,00,min}$ is calculated with Eq. (5) in the same way. The corresponding maximum and minimum state of charge can be calculated using the linearized characteristic curve of a battery defined by

$$SOC_{\{max,min\}} = \left(m \cdot U_{ES,00,\{max,min\}} - t\right) \cdot 100\% \tag{6}$$

The parameters m and t can be calculated from discharge curves, which can be found in the manufacturer data. As will be described later, for the tested batteries this linearization is possible between 10% and 90% SOC.

5.4. Driving test

As described in Section 4.2, the vehicle is driven by the battery during start-up of the DMFC system. Furthermore, Section 5.3 indicates that the battery is not operated at 100% SOC, but rather at a partial state of charge (pSOC). Therefore, the question is if the battery can cover the start-up in this case. The driving test was thus defined. The starting point was the maximum state of charge SOC_{max} as determined in Section 5.3. The battery was then loaded with the characteristic driving cycle (see Fig. 1). The experimental setup is the same as for the voltage limit test in Section 5.3. The test was finished when the minimum state of charge SOC_{min} was reached. The total amount of discharged energy E_{drive} was calculated and compared with $E_{start,min}$, the energy needed for the start-up phase. The battery passes the driving test, if

$$E_{drive} \geq E_{start,min} \tag{7}$$

is fulfilled. $E_{start,min}$ was calculated from the minimum energy density ED_{min} in Table 5 for a battery volume of 20 l (see Section 4.2), taking into consideration that only 50% of the total energy content of a battery is useable (see Section 6.3). The minimum energy $ED_{start,min}$ during start-up is 650 Wh.

5.5. Thermal behavior

For safety reasons (especially with lithium batteries) and lifetime, it is important to know the thermal behavior of the battery during operation in the DMFC hybrid system. For this test, the DMFC hybrid system in Fig. 2 was set up in a test rig. Therefore, the DMFC stack was simulated with a power source. The behavior of the driving motor was simulated with a power sink (acceleration and driving) and a power source (braking). The buck converter was controlled according to the control strategy in [28]. This system was then tested with the characteristic driving cycle (see Fig. 1). The temperature of the battery was measured. The battery fails the test if a maximum temperature is reached.

5.6. Lifetime test

As described in Section 5.3, the battery is not operated at 100% SOC, but rather at a partial state of charge (pSOC). Lead-acid batteries in particular will suffer under a sulfation of the negative plate as reported in [30] when they are operated on a pSOC between 30% and 70%. This will cause a rapid decrease in the lifetime. There are no overnight rest periods during operation of the vehicle (see Section 2). Therefore, it is not possible for prevention of sulfation to recharge the battery completely during these rest periods.

A procedure was developed to test the lifetime of batteries under pSOC operation. These tests were performed at the Institute for Power Electronics and Electrical Drives (ISEA) at RWTH Aachen University. The basis for the lifetime test was a test cycle, which consists of the following five steps:

- step 1: battery charge (2 h @ 100 A)
- step 2: repetition of test cycle A (see Fig. 6) until 30% of the nominal capacity has been discharged
- step 3: repetition of test cycle B (see Fig. 6) until the duration of step 2 and step 3 is 22 h
- step 4: 28 repetitions of steps 1 to 3
- step 5: capacity test (battery charge → battery discharge with 10 A)

The lifetime tests were performed in a special test rig, in which the tested battery is connected in parallel with a current source and a current sink. For step 1 the current source is used to charge the battery as defined. In step 2 and step 3 the current source and the current sink are used to load the battery with the defined cycles A and B. In step 5 firstly the battery is fully charged using the current source. Secondly the battery is discharged using the current sink.

Cycle A and cycle B in Fig. 6 are an approximation for the start-up and the normal operation of the DMFC system as described in section 4.2. During start-up the vehicle is only driven by the battery. Therefore, the battery load is described by the characteristic driving cycle in Fig. 1. Cycle A approximates the characteristic driving cycle by using constant current steps for the acceleration and the braking

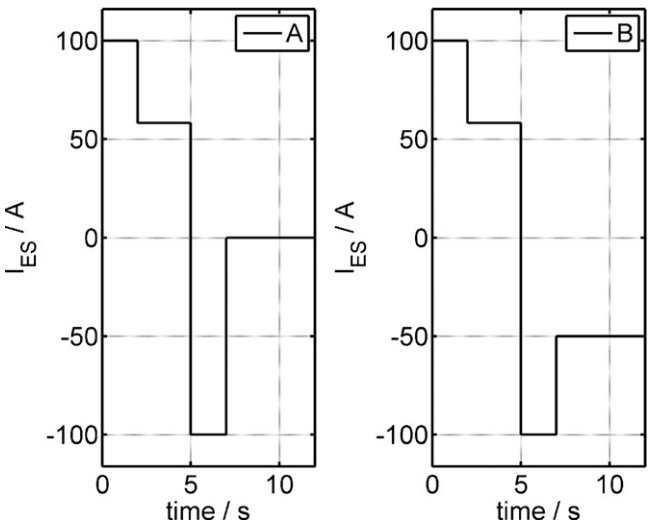

Fig. 6. Test cycle for lifetime test (battery current I_{ES}>0 for discharge and <0 for charge).

peak. The current steps are equal to the average current for a voltage of 24 V during acceleration and braking. The operation of the battery in step 2 is equal to the operation during start-up of the DMFC system. Different to cycle A is the last current step at −50 A in cycle B. This represents the battery charge by the DMFC stack during standstill of the vehicle. Therefore, cycle B is equal to the normal operation. During this approximated normal operation in step 3, the battery remains on a constant SOC. All five steps were repeated until the end of life (EOL) of the battery was reached, which is equal to a state of health (SOH) of 80% [29]. The number of repetitions is indicated with n. The capacity test in step 5 was performed to measure the actual capacity $C_{ES,n}$ of the battery. The SOH is thus defined as follows:

$$SOH_n = \frac{C_{ES,n}}{C_{ES,0}} \quad (8)$$

SOH_n is the state of health after n repetitions of the described procedure. The discharged capacity at that point is $C_{ES,n}$, whereas $C_{ES,0}$ defines the capacity discharged during a capacity test at the beginning of the lifetime test.

6. Energy storage characterization

6.1. Introduction

The Ragone chart in Fig. 4 indicates that several batteries fulfil the performance limits ED_{min} and PD_{min}. As described in Section 4.2, the battery has two main tasks: deliver acceleration peak power and store braking peak power. If we compare the operation mode of the battery in the DMFC hybrid system with the original traction battery, it becomes clear that the peak load of both is very similar. The only difference is that the traction battery is discharged during driving, whereas the battery in the DMFC system stays at a fixed state of charge. As the original traction battery was a lead-acid battery, the first battery that was characterized was also a lead-acid battery. There are some additional advantages associated with using a lead-acid battery in the DMFC hybrid system:

- 150 years of operational experience
- common battery in the field of light traction applications
- high availability on the market
- battery technology with lowest costs

Table 6
Characteristic battery data.

Characteristic data	Lead-acid battery	Lithium battery	
		A	B
Cell technology	Spiral-wound AGM separator	Cylindrical NCA cathode high power	Coffee-bag NMC cathode high energy
Number of cells	12s	7s	7s 2p
Nominal voltage	24 V	25.2 V	25.2 V
Rated capacity	50 Ah	45 Ah	80 Ah
Energy density	67.7 Wh l^{-1}	64.2 W l^{-1}	141.4 Wh l^{-1}
Power density	735.5 W l^{-1}	1543.6 W l^{-1}	518.5 Wh l^{-1}
Volume	18.6 l	17.8 l	16.2 l

As indicated in Fig. 4 lithium and NiMH batteries could also cope with the performance limits. Several battery manufacturers have been contacted to find a suitable battery. At the time when this work was done, it was not possible to find a suitable NiMH battery on the market. All offered NiMH batteries could not be integrated in the available space. However, two possible lithium batteries were identified.

The chosen lead-acid battery was a special spiral-wound battery with an absorbent glass mat (AGM) separator [31], which is predestinated for high peak currents. The characteristic data of this battery are indicated in Table 6 according to [32,33]. The energy density and the power density are greater than the performance limits in Table 5. As the system voltage should be 24 V (see Section 5.3), two 12 V battery blocks were connected in series.

The characteristic data of the two lithium batteries can also be seen in Table 6. The values for the energy and the power density were calculated from the density values of the single cells indicated in [34,35]. Compared with the performance limits in Table 5, it becomes clear that both batteries lie within the defined range. The energy density of lithium battery A is slightly lower than the limit of 65 Wh l^{-1}, but this small difference is tolerable. Lithium battery A uses high power cells (HP), whereas lithium battery B uses high energy cells (HE). As lithium battery B uses high energy cells, two strings of seven cells in series had to be connected in parallel (7s 2p) instead of only seven cells in series (7s) for lithium battery A. This was done to achieve a suitable power density. They also differ in the cathode material. Lithium battery A uses lithium–nickel–cobalt–oxide (NCA) for the positive electrode [34], whereas lithium battery B uses lithium–nickel–manganese–cobalt–oxide (NMC) [36].

6.2. Capacity test

To determine if the discharged energy E_{cap} depends on the discharge current I_{cap}, two capacity tests were performed with each of the three batteries: the first with a discharge current of around 10 A and the second with a rated discharge current of 1 C. The results are shown in Table 7. As can be seen, the discharged energy E_{cap} is very much dependent on the discharge current in the case of the lead-acid battery. This is a well known phenomenon for lead-acid batteries [37]. This also becomes clear when looking at the discharge curve in Fig. 7. Here, the battery voltage U_{ES} is plotted

Table 7
Results of the capacity test.

Battery	I_{cap} (A)	E_{cap} (Wh)	ED_{cap} (Wh l^{-1})
Lead-acid	9.4	735.5	39.5
	49.4	377.9	20.3
Lithium A	9.4	1009.5	56.7
	44.5	954.7	53.6
Lithium B	9.4	1993.5	123.1
	79.4	1920.5	118.5

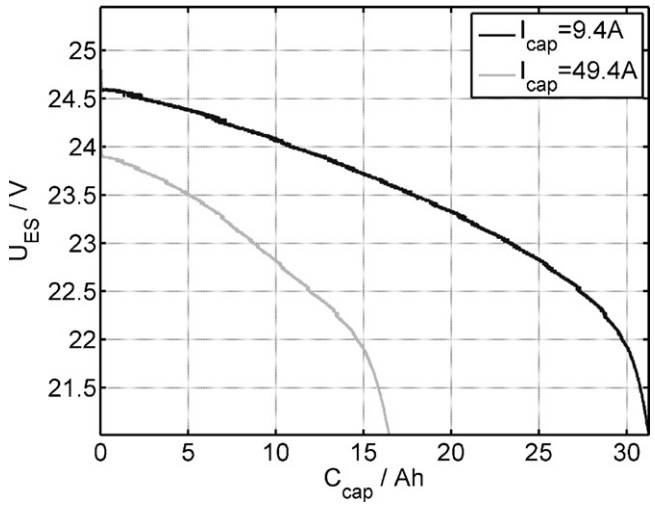

Fig. 7. Discharge curve for the lead-acid battery.

against the discharged battery capacity C_{cap} for both discharge currents. With the discharged energy E_{cap} in Table 7 and the battery volume in Table 6, a related energy density ED_{cap} can be calculated for each capacity test. Comparing the results in Table 7 with the performance limit ED_{min} in Table 5 reveals that the energy density derived from the capacity test is too small.

For the lithium batteries the dependency of the discharged energy E_{cap} on the discharge current is very small compared to the results for the lead-acid battery. This phenomenon is known for lithium batteries [37]. The difference between lithium and lead-acid batteries becomes clear when comparing the discharge curve of lithium battery A in Fig. 8 with the discharge curve of the lead-acid battery in Fig. 7. The discharge curve for lithium battery B is similar. The related energy densities for the capacity tests of the lithium batteries are also shown in Table 7. For lithium battery B, they are greater than the performance limit in Table 5. For lithium battery A, they are a bit lower, but the difference is tolerable.

6.3. Voltage limit test

The voltage limit test for all three batteries was performed as described in Section 5.3. Using Eqs. (4) and (5), it is possible to extract the following two dependencies from the measurements:

$$U_{ES,max} = f(U_{ES,00}) \tag{9}$$

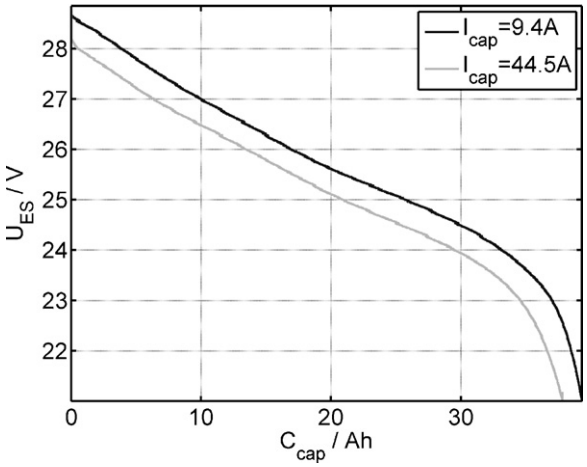

Fig. 8. Discharge curve for lithium battery A.

Table 8
Characteristic curve parameters.

Parameter	Lead-acid battery	Lithium battery	
		A	B
m	0.42 V^{-1}	0.19 V^{-1}	0.21 V^{-1}
t	9.90	4.58	4.95

$$U_{ES,min} = f(U_{ES,00}) \tag{10}$$

To obtain the dependency $f(SOC)$ for Eqs. (9) and (10), we used the linearized characteristic curve in Eq. (6) with the parameters m and t indicated in Table 8. These parameters were calculated with data from [31] for the lead-acid battery and from [34,35] for the lithium batteries. The results are shown in Figs. 9–11. Here $U_{ES,max}$ and $U_{ES,min}$ versus the SOC are plotted. The voltage limits $U_{level,max}$ and $U_{level,min}$ (see Section 5.3) are also shown.

The values for the two voltage limits $U_{level,max}$ and $U_{level,min}$ in the case of the lithium batteries were different to the voltage limits for the lead-acid battery. For the lithium batteries, the voltage range given by the driving motor (see Section 5.3) is not used, as both

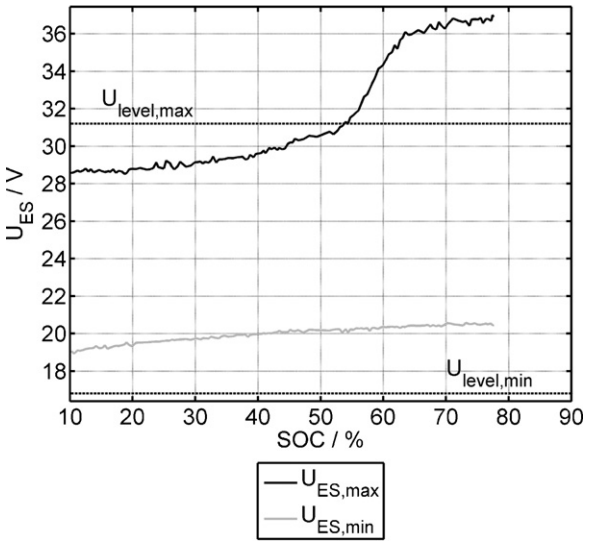

Fig. 9. Voltage limit test for the lead-acid battery.

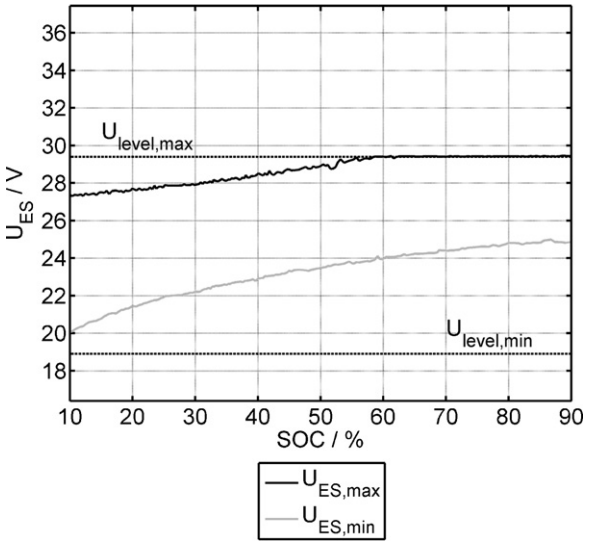

Fig. 10. Voltage limit test for lithium battery A.

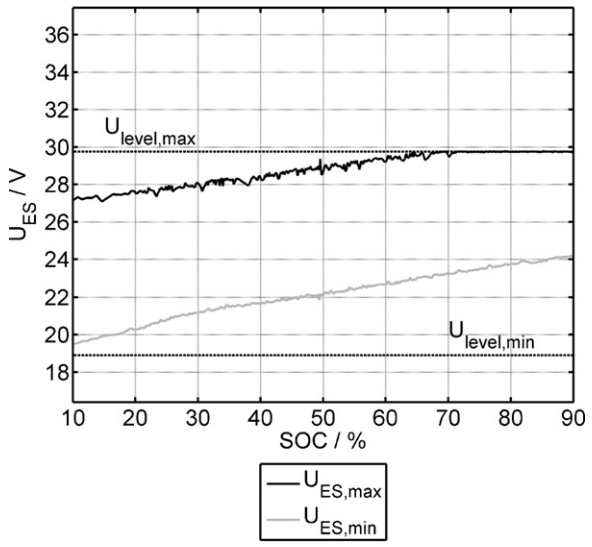

Fig. 11. Voltage limit test for lithium battery B.

lithium batteries are equipped with a battery management system (BMS), which has different maximum and minimum voltage limits for safety reasons. The maximum voltage level is particularly important to prevent lithium batteries from overcharge, which can lead to a thermal runaway resulting in a fire [38]. The voltage level values used here are shown in Table 9.

To obtain the maximum operating range of the batteries, Eqs. (4) and (5) were used to calculate the intersection between $U_{ES,max}$ and $U_{level,max}$ as well as the intersection between $U_{ES,min}$ and $U_{level,min}$. The results are shown in Table 10. As can be seen in Figs. 9–11, there is no intersection with the lower voltage limit $U_{level,min}$. Therefore, the minimum SOC level SOC_{min} is indicated with <10% in Table 10, as the linearized characteristic curve in Eq. (6) is only defined between 10% and 90% SOC. This means that all batteries are always able to deliver the maximum peak power during acceleration (see Table 1) without violating the lower voltage level $U_{level,min}$. For braking in contrast there is a limitation. Only for a partly discharged battery (SOC < 100%), it is possible to store the maximum braking power (see Table 1) in the battery without violating the upper voltage level $U_{level,max}$. All three batteries have to be operated on a partial state of charge (pSOC) in the DMFC hybrid system.

6.4. Driving test

The starting point for the driving test (see Section 5.4) is the maximum SOC indicated in Table 10. If each battery is loaded from that point with the characteristic driving cycle (see Fig. 1) until the minimum SOC in Table 10 is reached, it is possible to discharge an energy content E_{drive} as shown in Table 11. For the lead-acid battery this is only 42% of the minimum needed energy for start-up, which was determined in Section 5.4 as 650 Wh. As a consequence, it is not possible to cover the start-up phase of the DMFC system with this lead-acid battery. It becomes clear that the discharged energy of lithium battery B is more than needed. Lithium battery A is only able to deliver 82% of the needed energy. However, compared to the lead-acid battery this difference is acceptable.

Table 9
Voltage level values for the lithium batteries.

Voltage level	Lithium battery	
	A	B
$U_{level,max}$	29.4 V	29.8 V
$U_{level,min}$	18.9 V	18.9 V

Table 10
Maximum operating ranges.

SOC level	Lead-acid battery	Lithium battery	
		A	B
SOC_{max}	53.4%	58.3%	68.3%
SOC_{min}	<10%	< 10%	<10%

Table 11
Discharged driving energies.

	Lead-acid battery	Lithium battery	
		A	B
E_{drive}	273.6 Wh	529.9 Wh	1243.5 Wh

6.5. Thermal behavior

To test the thermal behavior, each battery was integrated into the DMFC hybrid system which was set up in a test rig as described in Section 5.5. During the test the temperature of the battery was measured. The temperature of the lead-acid battery reached a maximum value of 60 °C after an operating time of 2.5 h. The test was terminated at this point, as the real temperature in the single cells of the battery would be greater than the temperature measured at the housing. For a second test, the lead-acid battery was equipped with an axial fan for air cooling. The maximum temperature after 2.5 h was 40 °C but was still rising. As the thermal behavior of batteries is important in terms of safety and lifetime, the lead-acid battery failed this test. It is not possible to operate the DMFC system with this lead-acid battery over a long period of time.

Especially for lithium batteries the temperature is an important factor because of safety reasons. Therefore, both lithium batteries are equipped with an air cooling device. The integrated battery management system (BMS) controls the air blower according to the actual temperature. For lithium battery A it was shown that the temperature will always stay between 30 °C and 35 °C. This was demonstrated in a test with a duration of more than 200 h [23]. This leads to the conclusion that lithium battery A shows very stable thermal behavior. In contrast, lithium battery B showed a temperature increase from 25 °C to 50 °C in 5 h for the same test. Reaching 50 °C, the BMS disconnected the battery from the load. Afterwards, it took a long time to cool the battery down to 25 °C again. The cooling device of lithium battery B is thus not suitable for this kind of application and has to be optimized. A modified battery still needs to be tested.

6.6. Lifetime test

The lifetime test for the lead-acid battery was performed as described in Section 5.6. The results can be seen in Fig. 12. Here, the state of health (SOH) is plotted against the nominal capacity turnover. If a SOH of 80% defines the end of life of a battery, this is reached after 1443 nominal capacity turnovers. At that point it was possible to refresh the battery. This refresh consists of a charge process with a duration of 40 h and a charge current of 1 A. The SOH after this first refresh was >80% and the lifetime test was continued. The next refresh at 1882 nominal capacity turnovers was unsuccessful. Simulations were performed to get a feeling of how many operating hours correspond to the number of nominal capacity turnovers. These are described in detail in [23]. For the characteristic driving cycle in Fig. 1, we got 0.78 nominal capacity turnovers for an operating time of 1 h in the case of the lead-acid

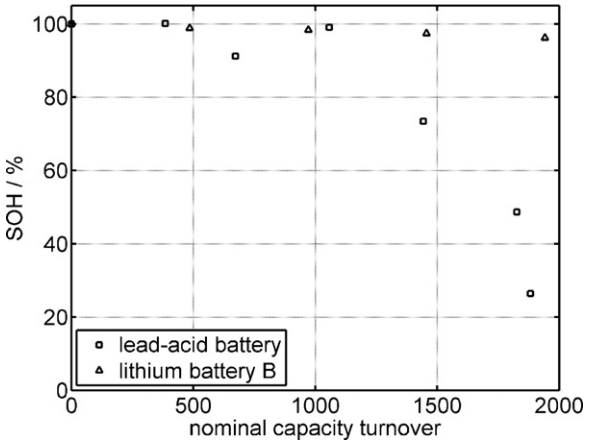

Fig. 12. Lifetime test for the lead-acid battery and lithium battery B.

battery. The 1443 nominal capacity turnovers at the first refresh corresponds to an operating time of 1850 h.

For the lithium batteries the lifetime test was performed exemplarily with lithium battery B. This test is still running. The first results are shown in Fig. 12. It can be seen that after 1940 nominal capacity turnovers, the SOH is still 96%. At this time, the end of life of the lead-acid battery was reached. Here the pSOC operation had no effect on the lifetime of lithium battery B. As this is a well-known phenomenon for lithium batteries [39], it is expected that lithium battery A will also have an increased lifetime compared to the lead-acid battery. This 1940 nominal capacity turnovers correspond to an operating time of 3970 h.

Obtaining a desired lifetime of 5000 h [8] for the complete DMFC hybrid system, the results of the lifetime test have the following consequences:

- refresh of the lead-acid battery at the end of life → disadvantage: needs a long time
- substitution of the lead-acid battery at the end of life → disadvantage: several sets of batteries are needed for the lifetime of the system
- another battery technology (e.g. lithium) → disadvantage: higher costs

6.7. Summary

In Section 5.1, several questions were defined to be answered during the battery characterization. The results of the battery characterization can be summarized as follows:

- The energy content of the lead-acid battery depends very much on the discharge current. In contrast, this dependency is very small for both lithium batteries.
- All batteries must be operated at a partial state of charge (pSOC).
- For pSOC operation, the energy content of the lead-acid battery is too small to cover the start-up. For the lithium batteries this energy content is sufficient.
- Thermal management for this kind of operation is very important.
- The pSOC operation results in an increased aging of the lead-acid battery, whereas this operation has no effect on a rapid decrease in lifetime of the lithium batteries.

6.8. Rating matrix

The characterization tests performed with one lead-acid battery and two lithium batteries were compared to each other. The results of this comparison can be displayed in a rating matrix (see Table 12). We recorded whether each battery passed (+) or failed (−) the different tests. If the test result was sufficient, it was marked with 0.

Table 12
Rating matrix for the battery characterization.

	Lead-acid battery	Lithium battery A	Lithium battery B
Capacity test	–	0	+
Voltage limit test	–	0	+
Driving test	–	0	+
Thermal behavior	–	+	–
Lifetime test	–	+	+

It can be clearly seen that the lead-acid battery is unsuitable for this kind of application. Lithium battery B showed the best results in all tests except the thermal behavior test. As lithium battery A successfully passed this test and also showed acceptable results in the other tests, this battery was chosen. Although no lifetime test was performed, better lifetimes are expected for lithium batteries in general. As a result, the DMFC hybrid system was constructed with lithium battery A [16]. This DMFC hybrid system was subjected to a long term test in a test rig with the characteristic driving cycle (see Fig. 1). This test lasted 2200 h. From time to time, a capacity test was performed for lithium battery A. At the end of the long term test, the SOH was nearly 100%. There was no aging of the battery, which proved the expected longer lifetime.

7. Conclusions

There are several advantages (e.g. faster refueling, extended operating time) in replacing the lead-acid battery in light traction applications with a DMFC system. A possible application is a horizontal order picker, the typical operation of which can be described with a characteristic driving cycle. Due to the highly fluctuating load profile, the DMFC stack has to be hybridized. In this case, an active series hybrid is the best solution. According to the requirements of the load profile, the DMFC stack and the energy storage are dimensioned in the run-up. It was shown that for this kind of application, a high energy density as well as a high power density is needed for the energy storage. When looking at different energy storage technologies, it becomes clear that super capacitors are not an option because of their low energy density. In contrast, some batteries have a high energy density and high power density. Three possible batteries (one lead-acid battery, two lithium batteries) were identified. To find the best battery for this application, a characterization procedure adapted to the requirements of the application was developed. The aim of this characterization was to analyze the behavior of the battery in the DMFC hybrid system. A capacity test with different discharge currents showed that especially for lead-acid batteries the energy content depends on the discharge current, whereas the energy content of lithium batteries is nearly independent. For use in the DMFC hybrid system, it is important that the battery voltage stays between defined voltage limits. A voltage limit test showed that all characterized batteries had to be operated at a pSOC between 50% and 70%. As the battery is operated at a pSOC, only part of the rated capacity can be used. This energy should be enough to operate the vehicle during start-up of the DMFC system. Only the two tested lithium batteries were able to cover the start-up. The battery temperature is an important factor especially for lithium batteries because of safety reasons. A thermal behavior test showed that cooling the batteries is very important. The identified pSOC operation could influence the lifetime of the battery. It was shown that the lead-acid battery undergoes accelerated aging under this operation, whereas the lifetime of lithium batteries is not influenced. As a result of all the characterization

tests, a lithium battery was identified as the best battery for use in the DMFC hybrid system.

References

[1] H. Dohle, J. Mergel, D. Stolten, J. Power Sources 111 (2002) 268–282.
[2] M. Nölke, Entwicklung, Auslegung und Umsetzung eines DMFC-Systems der kW-Klasse, Ph.D. thesis, RWTH Aachen University, 2007.
[3] D. Stolten, Hydrogen and Fuel Cells, vol. 1, Wiley–VCH Verlag, 2010, pp. 41–60.
[4] H. Janßen, L. Blum, N. Kimiaie, A. Maintz, J. Mergel, M. Müller, D. Stolten, Proceedings of the 3rd European PEFC Forum, Lucerne, Switzerland, 2005.
[5] Forschungszentrum Jülich, IEF-3 Report 2007: From basic principles to complete systems, Schriften des Forschungszentrums Jülich, Energy Technology, vol. 70, 2007, pp. 6–9.
[6] K. Steckmann, World Electric Vehicle J. 3 (2009).
[7] Yamaha, Proceedings of the 3rd International Hydrogen and Fuel Cell Expo and Seminar, Tokyo, Japan, 2007.
[8] J. Mergel, M. Müller, H. Janßen, D. Stolten, Proceedings of the 4. Deutscher Wasserstoffkongress, Essen, Germany, 2008.
[9] Jungheinrich, ECE 220 Horizontal order picker (2000 kg) (Datasheet), 2005.
[10] Industrial Truck Association, http://www.indtrk.org/products.asp?id=rmp (Last visited: 10.08.2010).
[11] Proton Motor Fuel Cell GmbH, http://www.proton-motor.de/forklifttruck.html (Last visited: 10.08.2010).
[12] Plug Power Inc., http://www.plugpower.com/products/materialhandlinggendrive (Last visited: 10.08.2010).
[13] Hydrogenics Corporation, http://www.hydrogenics.com/fuel/material_handling (Last visited: 10.08.2010).
[14] Nuvera Fuel Cells, http://www.nuvera.com/products/poweredge.php (Last visited: 10.08.2010).
[15] Oorja Protonics Inc., http://www.oorjaprotonics.com/oorja/OOrjapacOverview.php (Last visited: 10.08.2010).
[16] H. Janßen, L. Blum, M. Hehemann, J. Mergel, D. Stolten, Proceedings of the 18th World Energy Hydrogen Conference (WHEC 2010), Essen, Germany, 2010.
[17] J. Müller, K. Rotkopf, C. Sonntag, C. Böhm, P. Rabenseifner, Hybrid Power Source, United States Patent Application, US 2005/0249985 A1, 2005.
[18] R.M. Moore, S. Ramaswamy, J.M. Cunningham, K.H. Hauer, Fuel Cells 6 (2006) 387–402.
[19] O. Garcia, DC/DC-Wandler für die Leistungsverteilung in einem Elektrofahrzeug mit Brennstofftzellen und Superkondensatoren, Ph.D. thesis, ETH Zurich, 2002.
[20] W. Gao, IEEE Trans. Veh. Technol. 54 (2005) 846–855.
[21] A.R. Miller, J. Peters, B.E. Smith, O.A. Velev, J. Power Sources 157 (2006) 855–861.
[22] A. Di Napoli, F. Crescimbini, L. Solero, G. Pede, G.L. Bianco, M. Pasquali, Proceedings of the 18th International Electric Vehicle Symposium, Berlin, Germany, 2001.
[23] J. Wilhelm, Hybridisierung und Regelung eines mobilen Direktmethanol-Brennstoffzellen-Systems, Ph.D. thesis, RWTH Aachen University, 2010.
[24] K.S. Jeong, B.S. Oh, J. Power Sources 105 (2002) 58–65.
[25] A. Pesaran, M. Zolot, T. Markel, K. Wipke, Proceedings of the 9th Ulm Electrochemical Talks (UECT 2004), Ulm, Germany, 2004.
[26] M.J. Blackwelder, R.A. Dougal, J. Power Sources 134 (2004) 139–147.
[27] J. Wilhelm, L. Blum, H. Janßen, J. Mergel, D. Stolten, Proceedings of the 18th World Energy Hydrogen Conference (WHEC 2010), Essen, Germany, 2010.
[28] J. Wilhelm, L. Blum, H. Janßen, J. Mergel, D. Stolten, Proceedings of the 3rd European and International Conference eHydrogenia, Bucharest, Romania, 2009.
[29] A. Jossen, W. Weydanz, Moderne Akkumulatoren richtig einsetzen, vol. 1, print-yourbook Inge Reichardt Verlag, 2006.
[30] L.T. Lam, R. Louey, N.P. Haigh, O.V. Lim, D.G. Vella, C.G. Phyland, L.H. Vu, J. Furukawa, T. Takada, D. Monma, T. Kano, J. Power Sources 174 (2007) 16–29.
[31] M. Soria, F. Trinidad, J. Lacadena, J. Valenciano, G. Arce, J. Power Sources 174 (2007) 41–48.
[32] Exide Automotive Batterien, http://www.exide-automotive.de/produkte/maxxima/typenueber.html (Last visited: 27.05.2010).
[33] C. Andersson, On Auxiliary Systems in Commercial Vehicles, Ph.D. thesis, Lund University, 2004.
[34] GAIA, HP 602030 NCA - 45 Ah/162 Wh - Lithium Ion Cell (Datasheet), 2009.
[35] Li-Tec, HEI 40 High Energy Zelle ICNMP 110190240 (Datasheet), 2008.
[36] J. Kaiser, Proceedings of the 12th Ulm Electrochemical Talks (UECT 2010), Ulm, Germany, 2010.
[37] D. Doerffel, S.A. Sharkh, J. Power Sources 155 (2006) 395–400.
[38] A. Jossen, Proceedings of Energiespeicher für Bordnetze und Antriebssysteme (Haus der Technik), Essen, Germany, 2008.
[39] K. Kato, A. Negishi, K. Nozaki, I. Tsuda, K. Takano, J. Power Sources 117 (2003) 118–123.